Journal of Electronic Materials manuscript No.
(will be inserted by the editor)

W and X photoluminescence centers in crystalline Si: chasing candidates at atomic level through multiscale simulations

María Aboy · Iván Santos · Pedro López · Luis A. Marqués · Lourdes Pelaz

Received: date / Accepted: date

Abstract We combined several atomistic techniques to identify the structure of defects responsible for X and W photoluminescence lines in crystalline Si. We used kinetic Monte Carlo simulations to reproduce irradiation and annealing conditions used in photoluminescence experiments. We found that W and X radiative centers are related to small Si self-interstitial clusters but they coexists with larger Si self-interstitials clusters that can act as non-radiative centers. We used molecular dynamics simulations to explore the many different configurations of small Si self-interstitial clusters, and select those with the symmetry compatible to W and X photoluminescence centers. Using *ab initio* simulations we calculated their formation energy, donor levels and energy of local vibrational modes. On the ba-

M. Aboy · I. Santos · P. López · L. A. Marqués · L. Pelaz

Dpto. Electricidad y Electrónica, E.T.S.I. Telecomunicación, Universidad de Valladolid, Paseo Belén 15, 47011 Valladolid, Spain

Corresponding author: María Aboy

E-mail: marabo@tel.uva.es

sis of photoluminescence experiments and our theoretical multiscale calculations, we discuss the possible atomic configurations responsible for the W and X photoluminescence centers in Si. Our simulations also reveal that the intensity of photoluminiscence lines is the result of the competition between radiative centers and non-radiative competitors, which can explain the experimental quenching of the W and X lines even in the presence of the photoluminiscence centers.

Keywords photoluminescence and crystalline silicon and irradiation defect clusters and multiscale atomistic simulations

1 Introduction

The photoluminescence (PL) spectra of crystalline Si (c-Si) shows peaks with energies below the energy band gap associated to PL centers formed by defects involving dopants or impurities [1–3]. However, the origin of certain peaks remains unclear. Elucidating the nature of unknown PL centers can improve the capabilities of PL technique to identify lattice defects. Also, the possibility of converting Si into a sub-bandgap light-emitter semiconductor based on the introduction of PL centers has been explored [4, 5]. Among the PL lines with unclear origin, the W (1018 meV) and the less intense X (1040 meV) lines are observed after implantation at low dose, and their intensity can be maximized after subsequent thermal annealing or irradiating at elevated temperature (250-500°C) [6, 7].

The identification of the associated PL centers directly from experiments is difficult as irradiation generates a large variety of defects that coexist with these radiative defects. The intensity of a particular PL line depends on the capture of the photogenerated carriers by the PL centers in competition with other radiative

or non-radiative defects at their vicinity. From positron annihilation and photoluminescence experiments in ion implanted crystalline Si, Harding *et al.* proposed small vacancy clusters as possible non-radiative recombination centers responsible for the observed quenching of the W line as Si implant dose was increased [6, 8, 9]. In addition, in boron implanted crystaline Si samples, the interaction among dopant atoms and defects influenced the PL intensity of W and X lines [10]. This had been attributed to the formation of additional radiative [11] or non-radiative recombination centers [12] that compete in the capture of photogenerated carriers with the PL centers that existed on undoped samples. Despite this complex scenario, some features about defects responsible for W and X lines are known from experiments: they consist of Si self-interstitial clusters (I_n) [6, 7], the W center has trigonal symmetry while the X center has tetragonal symmetry [1–3], and their high energy local vibrational modes (LVMs) have been measured [1–3, 13]. In this work we use a multiscale simulation approach for exploring the possible structure of defects responsible for W and X lines through the comparison of these experimental evidences with the appropriate simulation technique.

2 Kinetic Monte Carlo simulations

We used non-lattice kinetic Monte Carlo (KMC) simulations to reproduce irradiation and annealing conditions used in PL experiments and to extract the relevant I_n size distribution. The simulation of implantation cascades was performed within the binary collision approximation, which provides the coordinates of Si self-interstitials, vacancies and implanted ions. This information is transferred to the KMC code for the simulation of the annealing at the implant temperature [14].

Interactions among defects and dopants have to be specified and their energetics (migration barriers, binding energies, etc) defined. In our simulations we use migration and formation energies for Si self-interstitials and vacancies reported in Ref. [14].

[Fig. 1 about here.]

The changes in the PL intensity of the W line under different irradiation conditions has been experimentally studied by Giri *et al.*[9]. They considered *c*-Si samples implanted with 80 keV Si ions at 265°C, conditions that are known to maximize the PL intensity of the W line [6, 7]. To provide understanding on the distribution of the W center, they varied the implant doses in the range of 10^{13}-$3 \cdot 10^{14}$ cm^{-2}, and afterwards they removed the implanted surface up to a depth of 200 and 255 nm. Figure 1(a) plots the PL intensity of the W line as a function of the implant dose for the as-implanted sample, as well as for 200 and 255 nm etched samples. These experiments show that the W-line intensity decreases with implant dose for the as-implanted sample. In contrast, after the surface removal, the PL intensity initially increases with implant dose and then saturates. Moreover, after the removal of the top surface, the PL intensity is lower than in the as-implanted sample for low implant doses, whereas for high implant doses it becomes higher than in the as-implanted sample.

We performed KMC simulations with the implant conditions of Giri's experiments, and we monitored the amount and distribution of I_n for each cluster size (n). Figure 1(b) plots the simulated I_n density of different sizes as a function of implant dose and Figs. 1(c) and (d) shows the simulated I_n depth distribution for 10^{13} and 10^{14} cm^{-2} implant doses, respectively. Our KMC simulations indicate

that the density of all I_n increases with implant dose (Fig.1(b)). However, it is worthy to note that the increment is more significant for larger clusters ($n > 6$) than for the smaller ones ($n \leq 5$). In principle, the experimentally observed decrease in the W-line PL intensity with implant dose in the as-implanted sample (Fig. 1(a)) should be associated with a decrease in the density of the I_n responsible for W PL with increasing implant dose. Our simulation results suggest that W line could be due to small I_n whereas larger clusters could act as non-radiative competitors. This hypothesis is compatible with the experimental changes in the PL intensity for the 255 nm etched sample compared to the as-implanted sample (Fig. 1(a)). Our simulations show that small I_n ($n \leq 5$) are dominant at the etched region for the low implant dose (Fig. 1(c)). Therefore, the reduction of the W-line PL intensity observed in experiments for 10^{13} cm^{-2} could be due to the removal of a high concentration of small I_n that could be responsible for the W line. In contrast, simulations show that for the higher implant dose (Fig. 1(d)) large I_n ($n > 6$) are dominant at the 255 nm etched region. Therefore, the increase in the W-line PL intensity reported in 255 nm etched samples at high implant doses could be due to the removal of a high percentage of large I_n that act as non-radiative competitors. Equivalent results are obtained from experiments studying the X PL line (not shown).

Previous works reported by Harding *et al.* [6, 8] proposed small vacancy clusters as quenching mechanism for the W line. These authors analyzed the implant conditions required to quench the PL intensity of the W line in 4 MeV Si implants in crystalline Si. A combination of PL measurements with the variable energy positron annihilation spectroscopy technique (which is only sensitive to vacancy defects) was used. These authors found a correlation between the quenching of the

W line and the concentration of small vacancy clusters in the vacancy-rich region typically obtained near the surface in ∼MeV implants [15]. We do not discard that small vacancy clusters act as non-radiative centers thus being responsible for the quenching of the PL intensity of the W line reported under the particular experimental conditions analyzed in that article. In the case of ∼keV implantation, as it is the case of the experiments considered in the present work [9], the different spatial separation among Si interstitial and vacancy distributions is less significant at the surface region. Our simulations show that the vacancy profile almost overlaps with the one for Si interstitials (not shown). We observed that the evolution of all vacancy clusters increases with implant dose in the whole damage profile for all the implant doses, being V_2 and V_3 clusters dominant. In contrast, for Si interstitial clusters (see Fig. 1(b)), the density of small Si interstitial clusters is dominant for low implant doses whereas the density of large Si interstitial clusters becomes comparable or even exceeds the density of the smaller ones as the implant dose increases. In addition, depth profiles show that these large clusters (which significantly increase their density with implant dose) are dominant in the surface region (0-250 nm) (see Fig. 1(c-d)). Therefore, our simulations suggest that the most significant difference between low and high implant doses as well as between no etched and etched samples lies in the presence of large Si interstitials clusters. For all these reasons, we proposed large Si interstitial clusters as candidates for non-radiative centers responsible for the quenching of the W line in the particular experiments reported by Giri *et al.* [9].

3 Classical molecular dynamics simulations

[Fig. 2 about here.]

On the basis of our KMC simulations, we assumed that W and X centers consist of small I_n ($n \leq 5$). However, the particular cluster size and structure of defects responsible for these PL lines can not be inferred from KMC simulations. We used classical molecular dynamics (CMD) simulations to explore the many different atomic configurations of small I_n ($n \leq 5$). In particular, we used the code LAMMPS [16], and we described Si-Si interactions using the Tersoff 3 empirical potential [17]. We introduced a number n of Si self-interstitials at neighboring positions in the simulation cells. We carried out annealing simulations at 1200 K during 25 ns, so the introduced defects form a I_n and its atomic configuration could evolve.

We found more than 100 configurations for I_n ($n \leq 5$) from atom dynamics, without assuming any pre-establish defect configuration. Among them, we selected those with the trigonal symmetry of the W center [2], and the tetragonal symmetry of the X center [3]. Selected configurations are shown in Fig. 2. For the W center, we have found a di-interstitial defect and a tri-interstitial cluster configuration previously reported by Carvalho *et al.*, known as I_3-V [18]. The di-interstitial defect has been labeled as I_2-V since it is very similar to the I_3-V defect configuration. It is worthy to note that the shown I_3-I tri-interstitial cluster was not obtained from our CMD simulations. As it was previously assigned to the W center by Carvalho *et al.* [18], we considered it in our analysis for completeness. For the X center, we have found a tri-interstitial defect previously reported by Bondi *et al.* [19], I_3-X in the following, and the tetra-interstitial cluster configuration proposed by Arai *et al.* [20] and considered as X center by Carvalho *et al.* [18], I_4-A in the following.

4 *Ab initio* simulations

[Fig. 3 about here.]

In order to determine whether our selected defects are compatible with radiative transistions of W and X centers an electronic description of the system is required, which was not affordable with the previous simulations techniques. We resorted to *ab initio* simulations to determine if the I_n selected from CMD simulations are compatible with radiative transitions of W and X centers. We used the VASP code [21, 22] with PBE-PAW pseudopotentials [23, 24] to characterize (i) the electronic band structure of defects, which shows whether a defect might favor or not radiative recombinations; (ii) the defect formation energy in order to obtain the defect levels within the energy band gap to relate them with experimental PL photon energies [25]; and (iii) the LVMs, which can be directly compared to the experimental values observed in PL spectra [26].

Since PL lines are associated to radiative recombinations, the electronic band structure of defects responsible for W and X PL lines should favor direct transitions. We represented in Fig. 3 the calculated electronic band structure of I_2-V and I_3-V defects, two of the candidates for the W center, along with the band structure of *c*-Si for comparison. The band structure of I_2-V shows two bands within the energy band gap, which discards it as a radiative center. For this reason, we will not consider I_2-V defect in the following discussion. In contrast, the band structure of I_3-V shows a new band at the top of the valence band, and the bottom of the conduction band is modified. These modifications in the electronic band structure with respect to *c*-Si suggests that direct transitions between band edges might be possible, and so might be radiative recombinations. The electronic band

structures of I_3-I, I_3-X and I_4-A (not shown) are also compatible with radiative recombinations.

[Table 1 about here.]

Table I summarizes other magnitudes calculated from *ab initio* simulations for those defects of Fig. 2 with band structure compatible with radiative transitions. For each defect, we report: (i) its formation energy for neutral charge state, $E_f[D^0]$; (ii) its donor level of defects, $E_{0/+}$, with respect to the valence band edge; and (iii) the energies of their LVMs, E_{Ph}. Details for these calculations can be found in Ref. [26]. It is worthy to note that I_3-I, considered by Carvalho *et al.* as W center, has the highest formation energy among I_3 defects considered in our study, and thus, it is the most unstable. In fact, I_3-I was not obtained from our CMD simulations, neither was it obtained in long-time tight-binding molecular dynamics simulations [27].

Regarding the energy levels introduced within the energy band gap, we found that defects considered in table I only have a $E_{0/+}$ donor level, but no $E_{0/-}$ acceptor level. We estimated the expected donor level of W and X PL centers from the energy difference between the c-Si band gap and the experimental photon energies (E_{PL}), as indicated in Eq. 1. The exciton binding energy is neglected in Eq. 1 as it is about one tenth of the carrier binding energy to the defect [28].

$$E_{0/+}^{expected} \simeq E_g(c\text{−Si}, \text{LowT}) - \text{E}_{\text{PL}} \tag{1}$$

Thus, the expected donor levels of W and X PL centers should be ~ 0.15 eV and ~ 0.13 eV, respectively, with respect to the valence band edge, considering an energy gap for c-Si close to 1.17 eV (as PL experiments are commonly performed at very low temperatures $\sim 4-20$ K). Results shown in table I indicate that I_3-V

is in better agreement with the donor level of the W center than I_3-I, while for the X center the better agreement is for I_3-X.

Finally, the LVMs of selected defects can be directly compared to the peaks that appear in the phonon-side bands of zero-phonon lines in PL spectra. Taking into account that GGA pseudopotentials tend to lower the energies of the LVMs [29], the better agreement among the defect candidates for the W center is for I_3-V, while for the X center both I_3-X and I_4-A show very similar values, which are slightly below experimental values.

5 Conclusions

We used a multiscale simulation approach to identify and characterize I_n configurations candidates to W and X photoluminescence centers in c-Si. We found that the so called I_3-V is the most likely candidate for W PL center. For the X center the so called I_3-X defect seems the most likely candidate, but we cannot be conclusive as not all its properties fit the experimental features within the accuracy of our calculations. Nevertheless, it should be noted that the evolution of W and X PL lines are not only the result of the evolution of the defects responsible for them. Other coexisting defects could act as non-radiative competitors that could quench the luminescence from the W and X photoluminescence centers in c-Si. Therefore, the optimization of the PL intensity involves not only the maximization of the radiative defect formation but also the removal of non-radiative defects.

Acknowledgements This work has been supported by EU (FEDER) and the Spanish Ministerio de Ciencia e Innovación under Project No. TEC2014-60694-P, and by the Junta de

Castilla y León under Project No. VA331U14. The authors thank the computational time provided by the Spanish Supercomputing Network through Project No. QCM-2014-3-0034.

References

1. G. Davies, Physics Reports **176**, 83 (1989)
2. G. Davies, E.C. Lightowlers, Z.E. Ciechanowska, J. Phys. C: Solid State Phys. **20**, 191 (1987)
3. Z.E. Ciechanowska, G. Davies, E.C. Lightowlers, Solid State Commun. **49**, 427 (1984)
4. J. Bao, M. Tabbal, T. Kim, S. Charnvanichborikarn, J.S. Williams, M.J. Aziz, F. Capasso, Opt. Express **15**, 6727 (2007)
5. S. Buckley, J. Chiles, A.N. McCaughan, G. Moody, K.L. Silverman, M.J. Stevens, R.P. Mirin, S.W. Nam, J.M. Shainline, Appl. Phys. Lett. **111**, 141101 (2017)
6. R.E. Harding, G. Davies, P.G. Coleman, C.P. Burrows, J. Wong-Leung, Phys. B **738**, 340 (2003)
7. B.C. Johnson, B.J. Villis, J.E. Burgess, N. Stavrias, J.C. McCallum, S. Charnvanichborikarn, J. Wong-Leung, C. Jagadish, J.S. Williams, J. Appl. Phys. **111**, 094910 (2012)
8. R.E. Harding, G. Davies, S. Hayama, P.G. Coleman, C.P. Burrows, J. Wong-Leung, Appl. Phys. Lett. **89**, 181917 (2006)
9. P.K. Giri, S. Coffa, E. Rimini, Appl. Phys. Lett. **78**, 291 (2001)
10. S. Charnvanichborikarn, B. Villis, B. Johnson, J. Wong-Leung, J. McCallum, J. Williams, C. Jagadish, Appl. Phys. Lett. **96**, 051906 (2010)

11. J. Adey, J.P. Goss, R. Jones, P.R. Briddon, Phys. Rev. B **67**, 245325 (2003)
12. M. Aboy, I. Santos, L. Pelaz, L. Marqués, P. López, 2011 IEEE Spanish Conf. on Electron Devices p. 051906 (2011)
13. S. Hayama, G. Davies, K.M. Itoh, J. Appl. Phys. **96**, 1754 (2004)
14. L. Pelaz, L.A. Marqués, M. Aboy, P. López, I. Santos, Eur. Phys. J. B **72**, 323 (2009)
15. S. Chakravarthi, S. Dunham, J. Appl. Phys. **89**, 4758 (2001)
16. S. Plimpton, J. Comp. Phys. **117**, 1 (1995). URL http://lammps.sandia.gov
17. J. Tersoff, Phys. Rev. B **38**, 9902 (1988)
18. A. Carvalho, R. Jones, J. Coutinho, P.R. Briddon, Phys. Rev. B **72**, 155208 (2005)
19. R. Bondi, S. Lee, G. Hwang, Phys. Rev. B **80**, 125202 (2009)
20. N. Arai, S. Takeda, M. Kohyama, Phys. Rev. Lett. **78**, 4265 (1997)
21. G. Kresse, J. Furthmuller, Comput. Mat. Sci. **6**, 15 (1996)
22. G. Kresse, J. Furthmuller, Phys. Rev. B **54**, 11169 (1996)
23. J.P. Perdew, K. Burke, M. Ernzerhof, Phys. Rev. Lett. **77**, 3865 (1996)
24. G. Kresse, D. Joubert, Phys. Rev. B **59**, 1758 (1999)
25. C. Freysoldt, B. Grabowski, T. Hickel, J. Neugebauer, G. Kresse, A. Janotti, C.V. de Walle, Rev. Mod. Phys. **86**, 253 (2014)
26. I. Santos, M. Aboy, P. López, L.A. Marqués, L. Pelaz, J. Phys. D: Appl. Phys. **49**, 075109 (2016)
27. D.A. Richie, J. Kim, S.A. Barr, K.R.A. Hazzard, R. Hennig, J.W. Wilkins, Phys. Rev. Lett. **92**, 045501 (2004)
28. I. Pelant, J. Valenta, *Experimental techniques of luminescence spectroscopy* (Oxford University Press, 2012), chap. 7, p. 186

29. F. Favot, A. Dal Corso, Phys. Rev. B **60**, 11427 (1999)

List of Figures

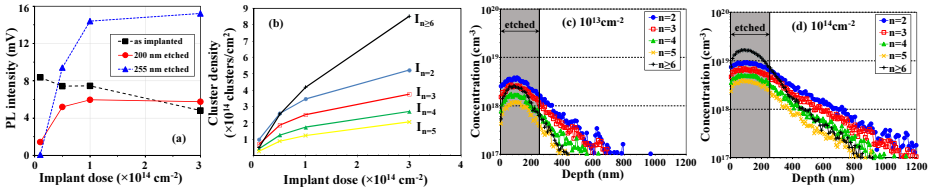

Fig. 1 (a) W-line PL intensity as a function of implant dose and etching depth (data were taken from Ref. [9]). (b) Density of I_n for different cluster sizes, n, after 80 keV Si at 265°C at several implant doses from KMC simulations, and (c-d) depth concentration profiles of I_n at those implantation conditions. Shadowed areas represent the 255 nm etched layer of Ref. [9]

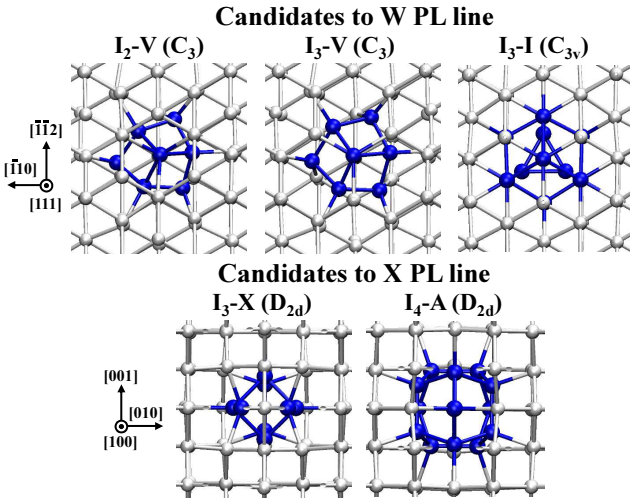

Fig. 2 Defects candidates to W (upper row) and X (lower row) PL centers. Atomic projection on convenient planes are shown to highlight their symmetry, which is indicated in parenthesis. Si lattice atoms and Si atoms of the defect are represented by white and blue spheres, respectively. Differences between I_2-V and I_3-V configurations are not evident in the selected projection. For more details see reference [26]

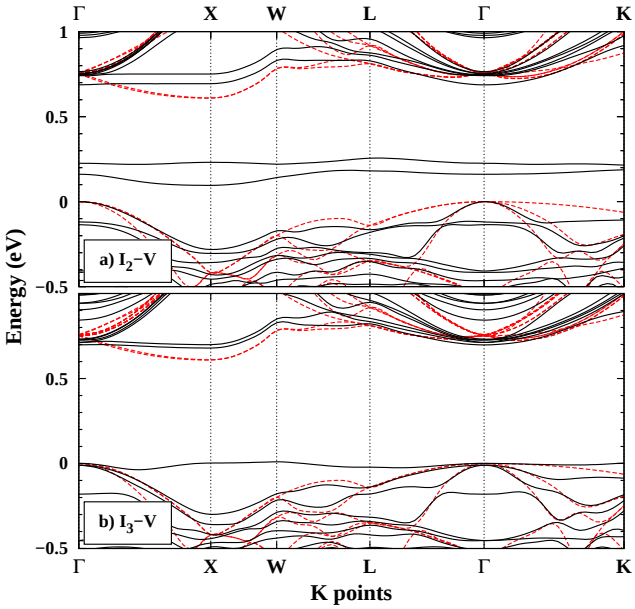

Fig. 3 Band structure modifications induced by (a) I_2-V and (b) I_3-V defects in their neutral charge state. Band structure of c-Si is also shown with red dashed lines for comparison.

List of Tables

Table I Properties of I_3-V, I_3-I, I_3-X and I_4-A from Fig. 2 obtained from *ab initio* simulations: formation energy for neutral configurations ($E_f[D^0]$), calculated and expected donor levels of defects ($E_{0/+}$) (see text for details), and high energy LVMs at the Γ point (E_{Ph}). Parentheses in E_{Ph} energies group LVMs with equivalent atomic movements.

Line	**Defect**	$\mathbf{E_f[D^0]}$**(eV)**	$\mathbf{E_{0/+}}$ **(eV)**		$\mathbf{E_{Ph}}$ **(meV)**	
			This work	Expected	This work	Experiments
W	I_3-V	6.74	0.13	~ 0.15	68.2, (59.9, 59.9)	70, 60, 56, 51 (Ref. [2])
	I_3-I	7.50	0.08		74.8, 74.8, 74.5, 70.8	
X	I_3-X	6.99	0.14	~ 0.13	62.8, 62.6, (61.6, 61.5)	69.0, 67.9, 66.2 (Ref. [13])
	I_4-A	7.42	0.19		63.6, (63.2, 63.2), 62.4	